

Current Biology

Pupil Size Coupling to Cortical States Protects the Stability of Deep Sleep via Parasympathetic Modulation

Highlights

- Infrared back-illumination allows accurate pupillometry in sleeping mice
- Brain activity and pupil diameter are tightly coupled during sleep
- The parasympathetic system is the main driver of pupillary changes during NREM sleep
- Pupillary constrictions might have a protective function to stabilize deep sleep

Authors

Özge Yüzgeç, Mario Prsa,
Robert Zimmermann, Daniel Huber

Correspondence

daniel.huber@unige.ch

In Brief

Using infrared back-illumination pupillometry in head-fixed sleeping mice, Yüzgeç et al. show that pupil diameter is tightly coupled to cortical states during sleep. Pharmacological and light-stimulation experiments reveal that the pupillary constrictions are parasympathetically driven and might have a protective function to stabilize deep sleep.



Pupil Size Coupling to Cortical States Protects the Stability of Deep Sleep via Parasympathetic Modulation

Özge Yüzgeç,^{1,2} Mario Prsa,^{1,2} Robert Zimmermann,^{1,2} and Daniel Huber^{1,3,*}

¹Department of Basic Neurosciences, University of Geneva, Geneva, Switzerland

²These authors contributed equally

³Lead Contact

*Correspondence: daniel.huber@unige.ch

<https://doi.org/10.1016/j.cub.2017.12.049>

SUMMARY

During wakefulness, pupil diameter can reflect changes in attention, vigilance, and cortical states. How pupil size relates to cortical activity during sleep, however, remains unknown. Pupillometry during natural sleep is inherently challenging since the eyelids are usually closed. Here, we present a novel head-fixed sleep paradigm in combination with infrared back-illumination pupillometry (iBip) allowing robust tracking of pupil diameter in sleeping mice. We found that pupil size can be used as a reliable indicator of sleep states and that cortical activity becomes tightly coupled to pupil size fluctuations during non-rapid eye movement (NREM) sleep. Pharmacological blocking experiments indicate that the observed pupil size changes during sleep are mediated via the parasympathetic system. We furthermore found that constrictions of the pupil during NREM episodes might play a protective role for stability of sleep depth. These findings reveal a fundamental relationship between cortical activity and pupil size, which has so far been hidden behind closed eyelids.

INTRODUCTION

Fluctuations in cortical states may determine learning efficiency, impact performance, and predict decisions [1–3]. Electrophysiological measurements, such as electrocorticograms (ECoGs), are reliable indicators of different cortical states and have as such been used to determine optimal conditions for sensory processing or cognitive performance [4]. Other physiological measurements, such as pupillometry, can be used as a non-invasive proxy for tracking vigilance states during behavior. Variations in pupil size can predict arousal [5], vigilance levels [6], and emotional responses [7] and reveal choice inclinations [8]. Due to its inexpensive and simple methodology, pupillometry has attracted not only the interest of neuroscientists, but also that of market researchers, athletes, and engineers. It became as such the focus for the development of practical applications, such as drowsiness detection while driving [9], fatigue [10],

and mental health assessments [11] or affective state classification [12].

More recently, studies in rodents and non-human primates have investigated interactions between cortical states and pupil diameter and found a close coupling during quiet wakefulness [13–15]. Follow-up studies combining optical imaging, electrophysiology, and modeling revealed that the link between brain activity and pupil diameter might be modulated by noradrenergic and cholinergic systems [16] and confirmed the occurrence of transient periods for optimal sensory processing.

Given the existing link between pupil size and cortical states during wakefulness, we asked whether a similar relationship persists during sleep. Changes in cortical states are very prominent during different sleep phases, while cognition- and sensory-related processes are strongly reduced. Would the pupil thus still fluctuate and what kind of changes would these fluctuations be related to during sleep? Might the pupil play a specific functional role, disturbance of which might interfere with sleep? In this study, we combined a novel approach allowing pupillometry in head-fixed naturally sleeping mice together with electrophysiology and pharmacology to find the answers to these questions.

RESULTS

Head-Fixed Sleeping Paradigm

The main challenge for pupil tracking during natural sleep is that mice often close their eyes, incline their head, or curl up (Figures 1A and 1B). Since pupil tracking is greatly facilitated during head-fixation as compared to freely moving conditions [17], we developed a setting allowing mice to fall asleep under head-fixed conditions. Using X-ray-based posture analysis, we adjusted the head angle and body position to mimic the body's natural position observed during quiet wakefulness and sleep (Figures 1B, 1C, and S1A; STAR Methods). Mice were gradually habituated to sleep in this position within 7 days in sound- and light-isolated boxes. ECoGs and electromyography (EMG; STAR Methods) of the neck muscle were used to monitor and quantify sleep states (Figure 1E). Recordings started while mice were awake and lasted up to 4 hr, most of which was spent in non-rapid eye movement (NREM) sleep with intermittent periods of rapid-eye movement (REM) sleep and wakefulness (awake) (Figure 1E). Similarly to sleeping mice in freely moving conditions [18, 19] (Figures S1B and S1C), awake states were characterized by high-amplitude, continuous EMG activity and high-frequency,



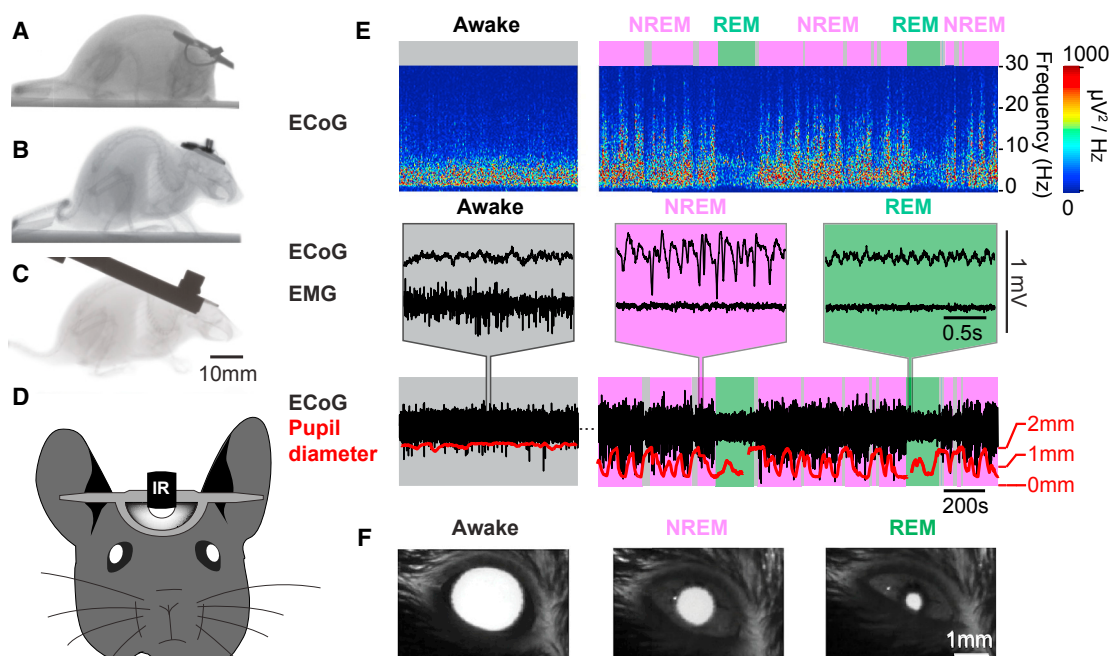


Figure 1. Head Fixed Sleep and iBip Pupil Tracking

(A) X-ray images of a naturally sleeping mouse in a curled-up position.

(B) Position of a sitting mouse during natural sleep.

(C) Head-fixed mouse with a head angle of 30 degrees.

(D) Front-view schematics of the infrared back-illumination pupillometry (iBip) pupil-tracking system. The 940 nm infrared light-emitting diode (LED) is placed above the skull, which allows the bright LED light to penetrate the head and back-illuminate the pupils.

(E) Top row: power spectrogram of M1 ECoG signal during awake, non-rapid eye movement (NREM) sleep, and rapid eye movement (REM) sleep states. Second row: a close-up of the ECoG and electromyography (EMG) signals during awake, NREM, and REM states. Third row: ECoG signal and pupil diameter during different cortical states. Data are from a habituated head-fixed mouse. The pupil diameter data are missing due to eye blinks at the beginning or end of REM periods.

(F) Images of pupil with infrared back illumination in awake, NREM and REM states.

See also [Figures S1](#) and [S2](#) and [Movie S1](#).

low-amplitude oscillations in the ECoG signal. NREM sleep was defined by high-amplitude ECoG and low or absent EMG activity. REM sleep was characterized by prominent ~ 7 Hz oscillations in the ECoG signal and complete disappearance of EMG activity (Figure 1E). Surprisingly, we found that head-fixed mice consistently sleep with their eyelids partially or fully open (Figure 1F), which allowed us to have access to the pupil diameter during continuous, natural-like sleep. Thus, we found that mice are able to sleep under head-fixed conditions, showing sleep patterns comparable to natural sleep under freely moving conditions (Figures S1B and S1C), yet with open eyelids [19, 20].

High-Contrast Infrared Back-Illumination Pupillometry

To enhance the contrast of the pupil for reliable tracking during head-fixed sleep, we developed infrared back-illumination pupillometry (iBip; see [STAR Methods](#)). For iBip, a 940 nm LED light source was placed on the skull of the mouse above frontal cortex, thereby illuminating the structures inside the head including the brain and the back of the eyes. When we imaged the eyes with infrared video cameras, the pupils appeared brightly illuminated (Figure 1F; [Movie S1](#)) and allowed reliable high-contrast tracking of their diameter and movement dynamics during natural sleep (Figures 1E, S2A, and S2B).

Pupil Size as an Identifier of Awake and Sleep Brain States

We first asked whether pupil diameter is qualitatively different during different sleep states. The average distribution of pupil size in darkness revealed that during the awake state, the pupil remains dilated most of the time (Figure 2A). During REM sleep (Figure S2B; [Movie S1](#)), it remains mostly constricted, whereas during NREM sleep, the pupil's diameter continually oscillates between small and large (Figure 2A). Plotting the median diameter versus its distribution width for each session yields three clearly separable clusters of points each corresponding to one of the three brain states (Figure 2A). Indeed, a K-means clustering analysis correctly partitioned 46 out of the 48 points into three sleep state categories.

The latter result implies that pupil size can be used as a reliable signal for brain state identification during sleep. To explicitly test this, we trained a neural network machine learning algorithm by providing the pupil diameter signal to its input layer and the sleep state label, identified based on the characteristics of corresponding ECoG and EMG signals, to the output layer. Each training trial consisted of a 100 s chunk of data, and we trained the neural network separately for each session by including datasets from all sessions but that one. The data of the remaining

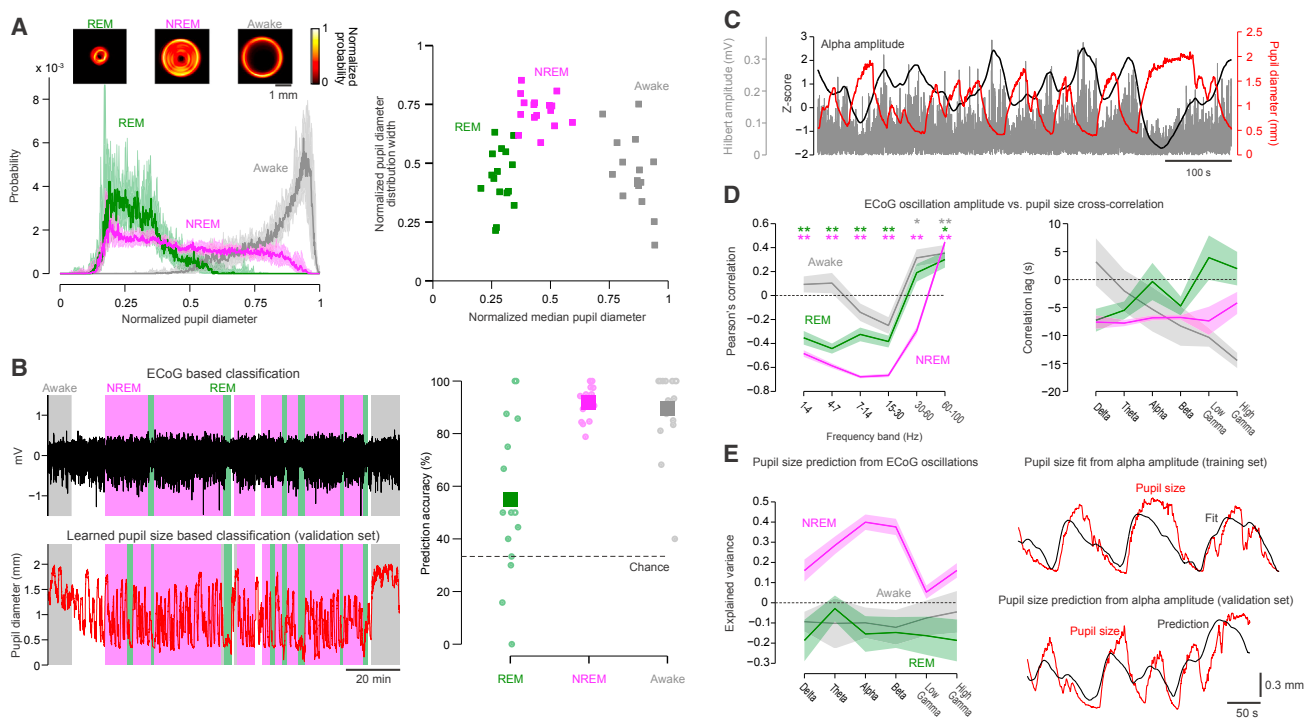


Figure 2. Pupil Size Fluctuations in Different Sleep States and Its Coupling to Brain Oscillations

(A) Left: median distribution (shaded regions are quartiles) of pupil diameter during REM, NREM, and awake states ($n = 16$ sessions). The pupil diameter has been normalized to its maximum recorded value in each experimental session. Insets show the location probability of the pupil's contour in one representative session for each state separately. Right: median pupil diameter versus its distribution width (the middle range containing 95% of the data points) of the 16 sessions. (B) Top: ECoG recording of an example session with the identified sleep states based on delta, theta, and EMG power classification criteria (see STAR Methods for details). Bottom: predicted sleep states based on the pupil diameter recording (red trace) of the same session using a trained neural network algorithm (see STAR Methods for details). Note that the episodes marked in white include mixed NREM and awake bouts shorter than 100 s and were therefore excluded. (C) Example session illustrating co-fluctuations of pupil size (red) and the Hilbert amplitude of ECoG oscillations in the alpha frequency band depicted in gray and its low-passed trace (denoted as alpha amplitude) in black.

(D) Mean (\pm SEM) Pearson's correlation between ECoG oscillatory magnitude of each frequency band and pupil diameter ($n = 16$ sessions) and the corresponding correlation lags, where negative values indicate that changes in oscillation size lead changes in pupil size. * $p < 0.01$, ** $p < 0.001$ (Student's *t* test, Bonferroni corrected).

(E) Left: mean (\pm SEM) variance accounted for between measured and predicted pupil size based on ECoG oscillations of each frequency band. Right: example session comparing the measured pupil size (red) to the fitted (top) and predicted (bottom) pupil size with a general linear model using alpha amplitude as a regressor.

See also Figure S2 and STAR Methods for details.

session was used to evaluate prediction accuracy. In this manner, the learned classification based on pupil diameter correctly predicted all three sleep states (Figure 2B) more often than expected by chance (REM: 58%, NREM: 96%, awake: 95%; REM: $p = 0.016$, NREM: $p < 0.001$, awake: $p < 0.001$, Wilcoxon signed-rank test). These results reveal that pupil size during natural sleep is a reliable identifier of different sleep states.

Co-variation of Pupil Size and Brain Oscillations

Temporal changes in pupil size were previously found to be tightly coupled to oscillations in bandlimited EEG power in awake animals [14–16]. We therefore asked whether such coupling is also present during sleep and how it differs between the different brain states. In order to test this, we looked at the correlation between pupillary activity and traditional brain rhythms [21–24]. Striking co-fluctuations of pupil size and amplitudes of bandlimited ECoG oscillations were indeed observed in sleeping mice (Figure 2C). This analysis revealed that the stron-

gest coupling is observed for the alpha (7 to 14 Hz) and beta (15 to 30 Hz) frequency bands (Figure 2D) in the NREM sleep state, where brain oscillations and pupil diameter are inversely correlated. Analysis at finer frequency resolution showed that peak negative correlation occurs in the spindle band (12 to 14 Hz; Figure S2C). Positive correlations were only found in the high-gamma band (60 to 100 Hz) and were similar in all three states. Brain oscillation changes led in time the changes in pupil size as indicated by the negative cross-correlation lags (Figure 2D).

To assess how steady these correlations are throughout a session in the different sleep states, we tested whether the oscillation amplitude can actually be used to predict pupil size ($n = 5$ mice). For each session, low-pass-filtered ECoG oscillation amplitudes were scaled to fit the pupil signal, and the fitted parameters were cross-validated on separate data of the same session (see STAR Methods). Surprisingly, only magnitude fluctuations of low-frequency oscillations (alpha and beta bands) during NREM sleep could reliably predict changes in pupil diameter

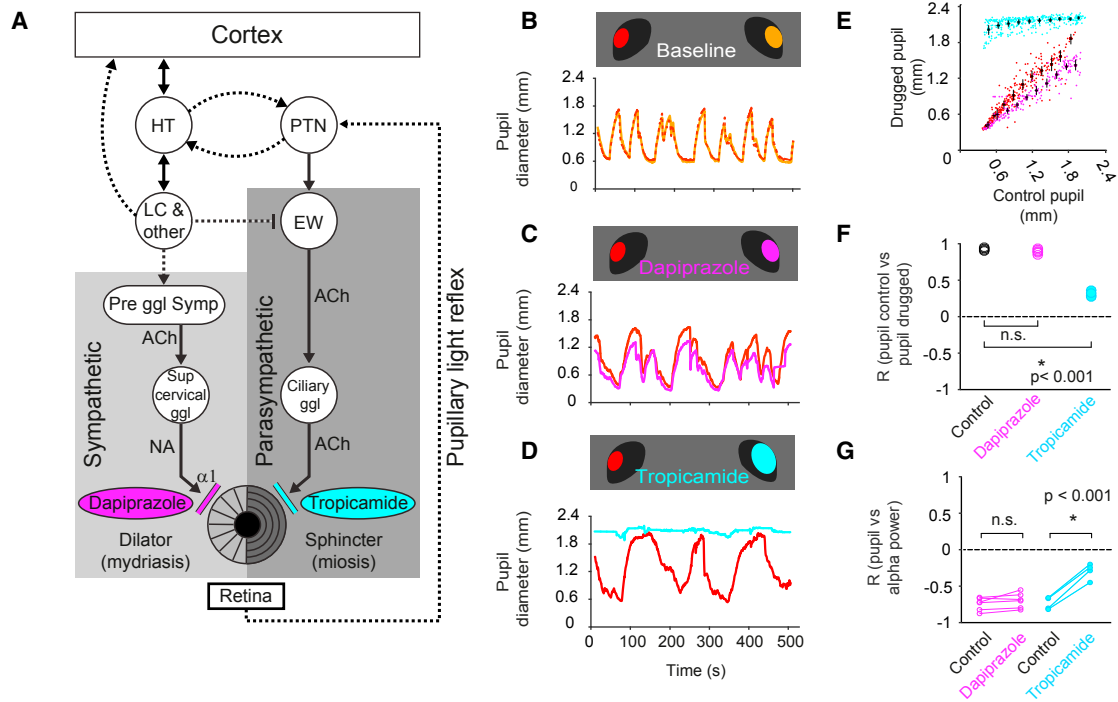


Figure 3. Mechanisms Underlying Coupling of Pupil Diameter and Brain Activity

(A) Schematics of the regulation of pupil size in relation to cortex through sympathetic and parasympathetic pathways (adapted from [28]).
 (B) Pupillary oscillations in both eyes in baseline condition in NREM sleep.
 (C) Pupillary oscillations in intact and dapiprazole-instilled eyes in NREM sleep.
 (D) Pupillary oscillations in intact and tropicamide-instilled eyes in NREM sleep.
 (E) Pupil size comparison of the eyes in baseline, dapiprazole-instilled, and tropicamide-instilled conditions in NREM sleep. Colored dots correspond to individual NREM bouts, and black dots are means (\pm SEM) of binned data (ten equally sized bins between the minimum and maximum size of the control pupil).
 (F) Cross-correlation of the pupil diameters in opposing eyes in NREM sleep in baseline, dapiprazole-instilled, and tropicamide-instilled conditions.
 (G) Cross-correlation of pupil diameter and the alpha power in the contralateral M1 in control, dapiprazole-instilled, and tropicamide-instilled conditions.
 See also [Figure S3](#) and [Movie S1](#).

(Figure 2E). Peak prediction accuracy was again observed to occur in the spindle band when the analysis was performed at a finer frequency resolution (Figure S2D). Given the inverse correlation, it follows that during NREM sleep, increases in the size of low-frequency brain oscillations predict pupil constrictions, and decreases predict pupil dilations. These two phenomena seem to reflect the fragile and deep sub-states of NREM sleep [25], respectively. These results also reveal that the covariation of cortical oscillations and pupil diameter is stronger during sleep as compared to the awake condition (Figure 2D) [14–16]. The fluctuations of pupil size and amplitude of ECoG oscillations were found to be periodic, with an infra-slow modulation frequency ranging from 0.01 to 0.02 Hz (Figures S2E–S2G). These infra-slow modulations have been shown to affect not only cortical activity, but also heartbeat [25, 26]. We indeed found that the changes in pupil diameter were positively correlated with changes in heart rate during NREM periods (Figure S3).

Mechanisms of Pupil Size Control in Sleep

During wakefulness, the pupil diameter is driven by an equilibrium of the sympathetic and parasympathetic systems [27]. Whereas the parasympathetic pathway mediates the constriction of the pupil during relaxation and upon light illumination, pu-

pil dilations during arousal or locomotion are mediated by the sympathetic system. In wakefulness, the sympathetic changes are closely coupled to cortical oscillations and are correlated with fluctuations in noradrenergic and cholinergic afferents [16]. The question therefore arises, is it the parasympathetic or the sympathetic system that mediates the tight coupling between pupil size and cortical states that we found to occur during sleep?

To assess their respective roles, we pharmacologically blocked the action of each of these two pathways at the level of the pupil. The sympathetic pathway was blocked by using an adrenergic alpha-1 receptor antagonist (dapiprazole), and the parasympathetic input to the pupil was inhibited by a cholinergic antagonist (tropicamide; Figure 3A). The drugs were applied to a single eye before the beginning of the sleep session, and the other eye was used as simultaneous control. To assess the effect of the drugs, we compared the correlation between ECoG in the alpha power band and pupil size in the NREM sleep state, which was found to be the most prominent co-fluctuation that exists between brain oscillations and pupil dynamics (Figure 2).

Under natural conditions, the pupils of the two eyes co-varied and were both correlated with the ECoG alpha power (Figures 3B, 3E, and 3G). Blocking the sympathetic afferents by

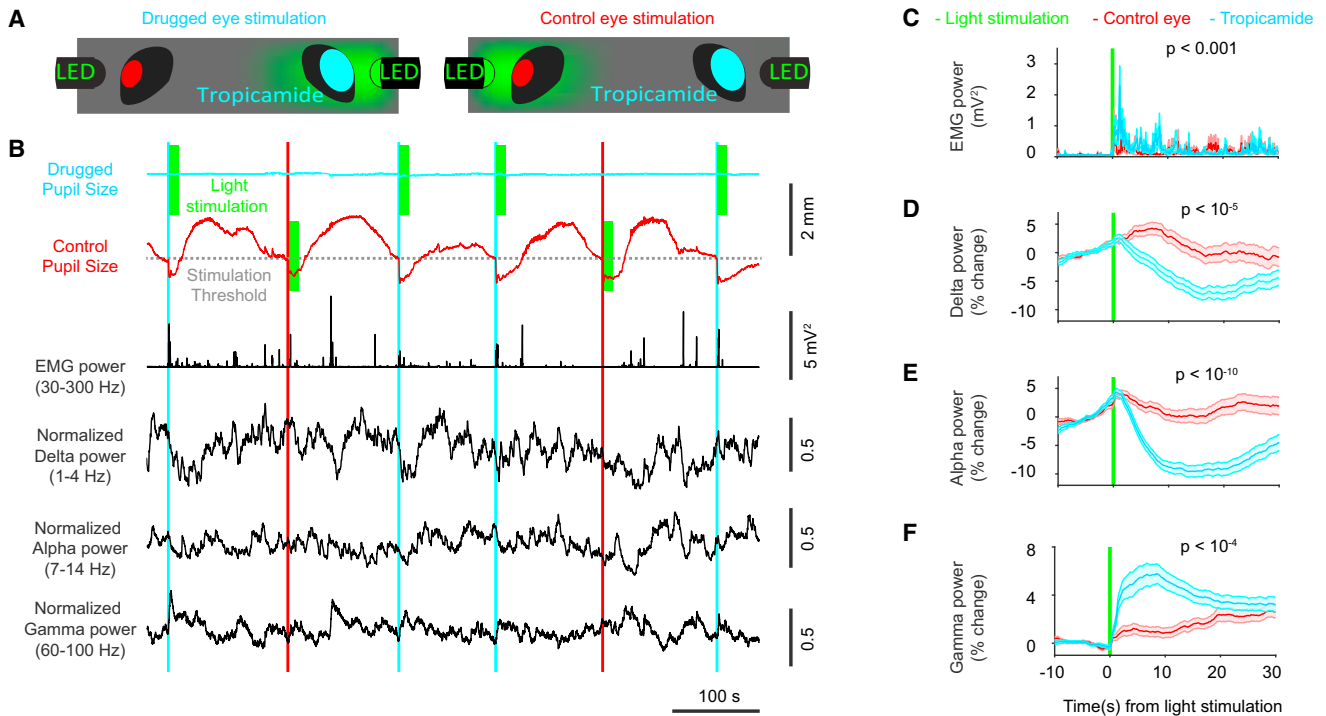


Figure 4. Potential Role of Pupillary Constrictions during NREM Sleep

(A) Schematics of the light-stimulation experiment.

(B) Pupil size traces of the drugged and control eyes with EMG and bandlimited ECoG power signals in a typical stimulation experiment. 1-s-long light stimulations are marked with green vertical bars on the pupil diameter traces.

(C) EMG activity at the time of light stimulation (two animals, 11 sessions, 196 control and 207 drugged-eye stimulation trials, mean \pm SEM) in C–F.

(D–F) Delta (D), alpha (E), and gamma (F) power change at the time of light stimulation.

application of dapiprazole led to a reduction of the maximum pupil diameter (Figures 3C–3F; $p < 10^{-10}$, Student's *t* test) but did not significantly change the correlation with the control eye pupil size (Figure 3F; $p = 0.61$, Student's *t* test) or with the power of alpha oscillations (Figure 3G; $p = 0.41$). In contrast, blocking the parasympathetic drive by tropicamide application dilated the pupil and removed its prominent fluctuations during NREM sleep (Figures 3D and 3F; $p < 10^{-6}$). More importantly, tropicamide treatment abolished the coupling that existed between pupil size and cortical activity (Figure 3G; $p < 0.001$). These results suggest that fluctuations in pupil diameter during sleep are mainly driven by the parasympathetic pathway.

As an independent measurement of the parasympathetic drive, we also monitored the heart rate (extracted from the EMG signal; see STAR Methods). We found that pupil diameter and heart rate are positively correlated during NREM sleep (Figure S3). These findings complement previous reports showing that heart rate is correlated with parasympathetic modulation and also with cortical activity during NREM sleep [25, 26, 29].

Potential Function of Pupil Size Changes during Sleep

Might the observed pupil size fluctuations be playing a functional role during sleep? For instance, could pupil constriction be acting as a protector from visual stimuli in order to preserve the stability of deep sleep? In order to investigate the potential protective function of pupil constrictions, we artificially dilated

one pupil with tropicamide, while leaving the other pupil intact as a control. The control pupil also allowed us to monitor the depth of NREM sleep (Figure 2). We then stimulated either the eye with the dilated pupil or the control eye with 1-s-long flashes of light (510 nm, 90 μ W) at the moment of putative deepest NREM sleep (i.e., at local minima of control pupil diameter and high alpha and delta power; see STAR Methods) [25] (Figure 4A). We simultaneously monitored the pupil diameters of both eyes, as well as EMG and ECoG activity (Figure 4B).

As expected, we found that briefly illuminating the control pupil caused a pupillary light reflex (Figure 4B), yet it only had a minor effect on the sleep state (Figures 4B–4F, red trace). In contrast, when the dilated pupil was illuminated with equal amounts of light, the animals showed robust signs of change in sleep states (Figures 4B–4F, blue trace). Besides the expected light-reflex-related constriction of the contra-lateral control pupil, the light stimulus triggered a sharp decrease in ECoG delta (Figure 4D; $p < 10^{-5}$, Student's *t* test) and alpha (Figure 4E, $p < 10^{-10}$) power, whereas it provoked significant increases in power in the high-gamma range (Figure 4F; $p < 10^{-4}$) and EMG activity (Figure 4C; $p < 0.001$, Wilcoxon rank-sum test). Given that high power in alpha and delta oscillations are associated with NREM sleep whereas high gamma power is associated with arousal [21], we conclude that light stimulation resulted in an arousal-like state change. These changes are reminiscent of state transitions toward arousal induced by brief optogenetic

manipulations [20, 30, 31]. Taken together, these results indicate that sleep states are altered differently upon sudden illumination depending on pupil size. We thus suggest that sustained pupil constrictions during deep sleep might have a protective role preventing light-induced wake-up.

DISCUSSION

Our study reveals that pupil size is dynamic during sleep and tightly coupled to the different sleep states. The deeper the sleep, the more the pupil constricts. This coupling is primarily mediated via the parasympathetic system and might provide a protective function by blocking visual input during deep sleep.

Pupil diameter and cortical states have been shown to be coupled to various degrees during wakefulness [13–15]. In our study, we show that cortico-pupillary coupling is enhanced during NREM compared to awake or REM states (Figure 2). We find that this correlation is strongest and negative in the alpha band (7 to 14 Hz, with a peak in the spindle band) and positive at higher frequencies (60 to 100 Hz) of cortical activity. This is consistent with previous reports during awake states in which the low alpha band (2 to 10 Hz) best predicted the decrease in sensory discrimination performance [15]. It is also reminiscent of recent reports in which slow fluctuations in the sigma range (10 to 15 Hz) were identified to best predict the depth and stability of NREM sleep [25, 32]. In the context of sleep versus wakefulness, this might also explain a higher correlation in our study compared to previous findings. We speculate that this tight coupling during sleep is not only due to the absence of external stimuli or locomotion, but is also related to the strong cyclical fluctuations of various neuronal and physiological parameters during NREM sleep, imposing a broad synchronicity on many processes.

The slow fluctuations in the ~ 0.01 to 0.02 Hz range found to pattern the alpha rhythm and pupil diameter during NREM sleep have previously been described across several species and brain regions. These infra-slow oscillations have been termed “cyclic alternating patterns” in humans [33], but they have also been found modulating the 10 to 15 Hz power in mice [25], the hippocampal EEG rhythms [34, 35], and activity in locus coeruleus neurons during sleep in mice [36]. Similar fluctuations and coupling with the pupil diameter have been reported during urethane anesthesia in rats [37]. Due to its ease of implementation and cost efficiency, monitoring pupil diameter with iBip thus provides a non-invasive and reliable handle (Figures 2A, 2B, and S2A) to this ultra-slow rhythm, facilitating the identification of sleep stages or fragility periods during natural sleep.

One of the potential origins of such infra-slow oscillations might be the suprachiasmatic nucleus (SCN) of the hypothalamus. The SCN shows prominent ~ 0.01 to 0.02 Hz oscillations [38, 39] and is connected to the main modulatory systems [40], which might alter cortical activity [16]. The SCN also has a direct and reciprocal connection with the pretectal nucleus (PTN) [41, 42], where the infra-slow oscillations are also observed [41–44] (Figure 3A). This pathway would provide a direct link to the parasympathetic modulation of the pupil via the Edinger-Westphal and the ciliary ganglion (Figure 3A). Alternatively, the thalamus has been suggested to modulate not only slow oscillations [45], but also alpha- and spindle-range activity in the cortex [46, 47]. Thalamic nuclei have been shown to oscillate at an infra-

slow rate [48] and to take part in maintaining the oscillations in SCN-PTN loop that impact pupillary constrictions [43]. Moreover, cholinergic activation of thalamic nuclei is reported to induce alpha rhythms [49]. Further experiments including subcortical recordings during sleep could reveal more about the role of different structures in generating infra-slow rhythms in the cortex and pupil size.

Blocking the sympathetic pathway with dapiprazole (an alpha adrenergic receptor antagonist) did not abolish the fluctuations or the correlation with ECoG oscillations (Figures 3C, 3F, and 3G). In contrast, tropicamide, a cholinergic blocker inhibiting the parasympathetic pathway to the pupil, significantly reduced the pupillary fluctuations and uncoupled them from the ECoG activity (Figures 3C, 3F, and 3G). Furthermore, we show that changes in the parasympathetically modulated heart rate [29] correlate positively to the pupillary oscillations in NREM sleep. These findings suggest that the observed dynamics of pupil diameter are not mediated by a decrease in sympathetic tone in the dilator muscle, but rather are mediated by an increase in the parasympathetic drive, causing an active pupil constriction during periods of deep sleep. Whether the cholinergic modulation of the pupil during NREM sleep is local or whether similar afferents can also affect other circuits, including the cortex, will have to be addressed in future experiments. The cholinergic tone in the brain is believed to be increase mostly during awake and REM states, yet there are reports of basal forebrain activity also in NREM sleep [50, 51].

How well these findings are applicable to other species, including humans, is not yet clear. Coupling of cortical activity and heart rhythm during sleep has been shown to be different in mice and humans [25, 26]. Also, blocking the parasympathetic input to the pupil was not sufficient to maintain complete dilations during sleep in children [52]. We can speculate that these inter-species differences might be due to differences in the balance of parasympathetic versus sympathetic drive during sleep or to different levels of baseline activity in autonomously regulated effector organs. The exact mechanism of how opposing autonomous systems act during sleep in both species remains an intriguing question for future sleep research.

This study was made possible by the fact that head-fixed mice can show an incomplete closure of their eyelids during natural sleep (nocturnal lagophthalmos). In humans, lagophthalmos can be caused by various conditions, including facial palsy (damage of the seventh nerve [53]). The reasons and mechanisms why this occurs in head-fixed sleeping mice are currently unclear. Anecdotally, we observed that the lagophthalmos decreased over weeks of repeated sleep sessions in some mice and might therefore be related to the habituation of the imposed body position. To reliably measure the pupil diameter during partial eyelid closure, we developed iBip. This technique was inspired by pupil tracking during *in vivo* two-photon calcium imaging, where the infrared light from the Ti Sapphire laser used for fluorophore excitation illuminates the back of the eyes [54]. The simplicity and low cost of iBip will most likely facilitate reliable pupil tracking in future studies during sleep and awake conditions. If used with higher frame rate (>60 Hz), iBip is ideally suited to track the eye movement dynamics during REM sleep (Figure S2B; Movie S1). Eye movements during tonic and phasic REM periods have been shown to have neural and muscular

correlates in adult and developing mammals [55–57]. Currently, the state-of-the-art rodent eye-tracking systems include implanted coils or electrodes around the eye area [57, 58]. Our technique would therefore provide a simple and noninvasive alternative for REM sleep studies.

Finally, we provide the first evidence for the protective role of pupil constrictions during sleep. Although eyelids have primarily a protective function, they still transmit light sufficiently [59] to cause changes in cortical states [60]. Light stimulus into the pharmacologically dilated eye during NREM sleep resulted in a change in ECoG and EMG signals that were similar to state transitions toward arousal induced by brief optogenetic manipulations [20, 30, 31] (Figures 4D–4F). In contrast, light stimulation to the control eye had only a minor effect on sleep states. Until recently, one of the primary mechanisms for regulating cortex and sensory stimuli interaction during sleep was thought to be the thalamic gating hypothesis [61] (but see [60, 62]). Our study provides an additional, periphery-dependent gating mechanism for protecting the brain from waking up during phases of deep sleep. We hypothesize that pupillary constriction might ensure the continuity of NREM sleep periods [25], which is considered to be critical for memory consolidation [20, 63].

STAR★METHODS

Detailed methods are provided in the online version of this paper and include the following:

- KEY RESOURCES TABLE
- CONTACT FOR REAGENT AND RESOURCE SHARING
- EXPERIMENTAL MODEL AND SUBJECT DETAILS
- METHOD DETAILS
 - Surgeries
 - Handling and sleep training
 - X-Ray imaging
 - Electrophysiology
 - Heart beat detection
 - Pupil tracking with iBip
 - Pharmacology and light stimulation experiments
- QUANTIFICATION AND STATISTICAL ANALYSIS
 - Sleep state classification
 - Pupil diameter detection
 - Pupil-based sleep state classification
 - Relating ECoG oscillations to pupil size fluctuations
 - Changes in ECoG signals with light stimulation

SUPPLEMENTAL INFORMATION

Supplemental Information includes three figures and one movie and can be found with this article online at <https://doi.org/10.1016/j.cub.2017.12.049>.

ACKNOWLEDGMENTS

We thank Gregorio Galñanes for insightful discussions, Anita Lüthi and Antoine Adamantidis for their advice and comments on the manuscript, and all members of the Huber lab for their support. This research was supported by the Swiss National Science Foundation (PP00P3_133710), European Research Council (OPTOMOT), New York Stem Cell Foundation, and International Foundation for Paraplegia Research. D.H. is a New York Stem Cell Foundation-Robertson Investigator.

AUTHOR CONTRIBUTIONS

O.Y., R.Z., and D.H. conceived the study. R.Z. developed the head-fixed sleep paradigm, conducted pilot head-fixed sleep experiments including the X-ray analysis, and discovered the coupling between pupil diameter and cortical activity. O.Y. conducted all experiments described in this paper including the design of pharmacology and stimulation experiments. O.Y. and R.Z. manually scored the data. O.Y. and M.P. analyzed the data. M.P. developed the video-acquisition and pupil-size-tracking systems. O.Y., M.P., and D.H. wrote the paper.

DECLARATION OF INTEREST

The authors declare no competing interests.

Received: October 4, 2017

Revised: December 1, 2017

Accepted: December 21, 2017

Published: January 18, 2018

REFERENCES

1. Eldar, E., Cohen, J.D., and Niv, Y. (2013). The effects of neural gain on attention and learning. *Nat. Neurosci.* *16*, 1146–1153.
2. Hesselmann, G., Kell, C.A., Eger, E., and Kleinschmidt, A. (2008). Spontaneous local variations in ongoing neural activity bias perceptual decisions. *Proc. Natl. Acad. Sci. USA* *105*, 10984–10989.
3. Cohen, M.R., and Maunsell, J.H.R. (2010). A neuronal population measure of attention predicts behavioral performance on individual trials. *J. Neurosci.* *30*, 15241–15253.
4. Aston-Jones, G., and Cohen, J.D. (2005). An integrative theory of locus coeruleus-norepinephrine function: adaptive gain and optimal performance. *Annu. Rev. Neurosci.* *28*, 403–450.
5. Bradley, M.M., Miccoli, L., Escrig, M.A., and Lang, P.J. (2008). The pupil as a measure of emotional arousal and autonomic activation. *Psychophysiology* *45*, 602–607.
6. Ebitz, R.B., Pearson, J.M., and Platt, M.L. (2014). Pupil size and social vigilance in rhesus macaques. *Front. Neurosci.* *8*, 100.
7. Partala, T., and Surakka, V. (2003). Pupil size variation as an indication of affective processing. *Int. J. Hum. Comput. Stud.* *59*, 185–198.
8. de Gee, J.W., Knapen, T., and Donner, T.H. (2014). Decision-related pupil dilation reflects upcoming choice and individual bias. *Proc. Natl. Acad. Sci. USA* *111*, E618–E625.
9. Nishiyama, J., Tanida, K., Kusumi, M., and Hirata, Y. (2007). The pupil as a possible premonitor of drowsiness. *Conf. Proc. IEEE Eng. Med. Biol. Soc.* *2007*, 1586–1589.
10. Morad, Y., Lemberg, H., Yofe, N., and Dagan, Y. (2000). Pupillography as an objective indicator of fatigue. *Curr. Eye Res.* *21*, 535–542.
11. Steidtmann, D., Ingram, R.E., and Siegle, G.J. (2010). Pupil response to negative emotional information in individuals at risk for depression. *Cogn. Emotion* *24*, 480–496.
12. Onorati, F., Barbieri, R., Mauri, M., Russo, V., and Mainardi, L. (2013). Characterization of affective states by pupillary dynamics and autonomic correlates. *Front. Neuroeng.* *6*, 9.
13. Reimer, J., Froudarakis, E., Cadwell, C.R., Yatsenko, D., Denfield, G.H., and Tolias, A.S. (2014). Pupil fluctuations track fast switching of cortical states during quiet wakefulness. *Neuron* *84*, 355–362.
14. Vinck, M., Batista-Brito, R., Knoblich, U., and Cardin, J.A. (2015). Arousal and locomotion make distinct contributions to cortical activity patterns and visual encoding. *Neuron* *86*, 740–754.
15. McGinley, M.J., David, S.V., and McCormick, D.A. (2015). Cortical Membrane Potential Signature of Optimal States for Sensory Signal Detection. *Neuron* *87*, 179–192.

16. Reimer, J., McGinley, M.J., Liu, Y., Rodenkirch, C., Wang, Q., McCormick, D.A., and Tolia, A.S. (2016). Pupil fluctuations track rapid changes in adrenergic and cholinergic activity in cortex. *Nat. Commun.* **7**, 13289.
17. Wallace, D.J., Greenberg, D.S., Sawinski, J., Rulla, S., Notaro, G., and Kerr, J.N. (2013). Rats maintain an overhead binocular field at the expense of constant fusion. *Nature* **498**, 65–69.
18. Weber, F., and Dan, Y. (2016). Circuit-based interrogation of sleep control. *Nature* **538**, 51–59.
19. Franken, P., Malafosse, A., and Tafti, M. (1999). Genetic determinants of sleep regulation in inbred mice. *Sleep* **22**, 155–169.
20. Rolls, A., Colas, D., Adamantidis, A., Carter, M., Lanre-Amos, T., Heller, H.C., and de Lecea, L. (2011). Optogenetic disruption of sleep continuity impairs memory consolidation. *Proc. Natl. Acad. Sci. USA* **108**, 13305–13310.
21. Buzsáki, G., and Draguhn, A. (2004). Neuronal oscillations in cortical networks. *Science* **304**, 1926–1929.
22. Steriade, M. (2006). Grouping of brain rhythms in corticothalamic systems. *Neuroscience* **137**, 1087–1106.
23. da Silva, F.H., van Lierop, T.H.M.T., Schrijver, C.F., and van Leeuwen, W.S. (1973). Organization of thalamic and cortical alpha rhythms: spectra and coherences. *Electroencephalogr. Clin. Neurophysiol.* **35**, 627–639.
24. Csicsvari, J., Jamieson, B., Wise, K.D., and Buzsáki, G. (2003). Mechanisms of gamma oscillations in the hippocampus of the behaving rat. *Neuron* **37**, 311–322.
25. Lecci, S., Fernandez, L.M.J., Weber, F.D., Cardis, R., Chatton, J.-Y., Born, J., and Lüthi, A. (2017). Coordinated infraslow neural and cardiac oscillations mark fragility and offline periods in mammalian sleep. *Sci. Adv.* **3**, e1602026.
26. Mensen, A., Zhang, Z., Qi, M., and Khatami, R. (2016). The occurrence of individual slow waves in sleep is predicted by heart rate. *Sci. Rep.* **6**, 29671.
27. Loewenfeld, I., and Lowenstein, O. (1999). *The Pupil: Anatomy, Physiology, and Clinical Applications* (Butterworth-Heinemann).
28. Hou, R.H., Samuels, E.R., Langley, R.W., Szabadi, E., and Bradshaw, C.M. (2007). Arousal and the pupil: why diazepam-induced sedation is not accompanied by miosis. *Psychopharmacology (Berl.)* **195**, 41–59.
29. Boudreau, P., Yeh, W.-H., Dumont, G.A., and Boivin, D.B. (2013). Circadian variation of heart rate variability across sleep stages. *Sleep* **36**, 1919–1928.
30. Adamantidis, A.R., Zhang, F., Aravanis, A.M., Deisseroth, K., and de Lecea, L. (2007). Neural substrates of awakening probed with optogenetic control of hypocretin neurons. *Nature* **450**, 420–424.
31. Herrera, C.G., Cadavieco, M.C., Jego, S., Ponomarenko, A., Korotkova, T., and Adamantidis, A. (2016). Hypothalamic feedforward inhibition of thalamocortical network controls arousal and consciousness. *Nat. Neurosci.* **19**, 290–298.
32. McKinney, S.M., Dang-Vu, T.T., Buxton, O.M., Solet, J.M., and Ellenbogen, J.M. (2011). Covert waking brain activity reveals instantaneous sleep depth. *PLoS ONE* **6**, e17351.
33. Parrino, L., Ferri, R., Bruni, O., and Terzano, M.G. (2012). Cyclic alternating pattern (CAP): the marker of sleep instability. *Sleep Med. Rev.* **16**, 27–45.
34. Buzsáki, G. (1986). Hippocampal sharp waves: their origin and significance. *Brain Res.* **398**, 242–252.
35. Penttonen, M., Nurminen, N., Miettinen, R., Sirviö, J., Henze, D.A., Csicsvári, J., and Buzsáki, G. (1999). Ultra-slow oscillation (0.025 Hz) triggers hippocampal afterdischarges in Wistar rats. *Neuroscience* **94**, 735–743.
36. Takahashi, K., Kayama, Y., Lin, J.S., and Sakai, K. (2010). Locus coeruleus neuronal activity during the sleep-waking cycle in mice. *Neuroscience* **169**, 1115–1126.
37. Blasiak, T., Zawadzki, A., and Lewandowski, M.H. (2013). Infra-slow oscillation (ISO) of the pupil size of urethane-anaesthetised rats. *PLoS ONE* **8**, e62430.
38. Miller, J.D., and Fuller, C.A. (1992). Isoperiodic neuronal activity in suprachiasmatic nucleus of the rat. *Am. J. Physiol.* **263**, R51–R58.
39. Aggelopoulos, N.C., and Meissl, H. (2000). Responses of neurones of the rat suprachiasmatic nucleus to retinal illumination under photopic and scotopic conditions. *J. Physiol.* **523**, 211–222.
40. Aston-Jones, G., Chen, S., Zhu, Y., and Oshinsky, M.L. (2001). A neural circuit for circadian regulation of arousal. *Nat. Neurosci.* **4**, 732–738.
41. Moga, M.M., and Moore, R.Y. (1997). Organization of neural inputs to the suprachiasmatic nucleus in the rat. *J. Comp. Neurol.* **389**, 508–534.
42. Krout, K.E., Kawano, J., Mettenleiter, T.C., and Loewy, A.D. (2002). CNS inputs to the suprachiasmatic nucleus of the rat. *Neuroscience* **110**, 73–92.
43. Szkudlarek, H.J., Herdizina, O., and Lewandowski, M.H. (2008). Ultra-slow oscillatory neuronal activity in the rat olivary pretectal nucleus: comparison with oscillations within the intergeniculate leaflet. *Eur. J. Neurosci.* **27**, 2657–2664.
44. Szkudlarek, H.J., Orlowska, P., and Lewandowski, M.H. (2012). Light-induced responses of slow oscillatory neurons of the rat olivary pretectal nucleus. *PLoS ONE* **7**, e33083.
45. Crunelli, V., and Hughes, S.W. (2010). The slow (<1 Hz) rhythm of non-REM sleep: a dialogue between three cardinal oscillators. *Nat. Neurosci.* **13**, 9–17.
46. De Gennaro, L., and Ferrara, M. (2003). Sleep spindles: an overview. *Sleep Med. Rev.* **7**, 423–440.
47. Lorincz, M.L., Kékesi, K.A., Juhász, G., Crunelli, V., and Hughes, S.W. (2009). Temporal framing of thalamic relay-mode firing by phasic inhibition during the alpha rhythm. *Neuron* **63**, 683–696.
48. Hughes, S.W., Lőrincz, M.L., Parri, H.R., and Crunelli, V. (2011). Infraslow (<0.1 Hz) oscillations in thalamic relay nuclei basic mechanisms and significance to health and disease states. *Prog. Brain Res.* **193**, 145–162.
49. Lőrincz, M.L., Crunelli, V., and Hughes, S.W. (2008). Cellular dynamics of cholinergically induced alpha (8–13 Hz) rhythms in sensory thalamic nuclei in vitro. *J. Neurosci.* **28**, 660–671.
50. Lőrincz, M.L., Gunner, D., Bao, Y., Connelly, W.M., Isaac, J.T.R., Hughes, S.W., and Crunelli, V. (2015). A distinct class of slow (~0.2–2 Hz) intrinsically bursting layer 5 pyramidal neurons determines UP/DOWN state dynamics in the neocortex. *J. Neurosci.* **35**, 5442–5458.
51. Hangya, B., Ranade, S.P., Lorenc, M., and Kepecs, A. (2015). Central cholinergic neurons are rapidly recruited by reinforcement feedback. *Cell* **162**, 1155–1168.
52. Krastel, H., Alexandridis, E., and Rating, D. (1996). [Sleep modifies anticholinergic mydriasis]. *Ophthalmologie* **93**, 476–478.
53. Pereira, M.V., and Glória, A.L. (2010). Lagophthalmos. *Semin. Ophthalmol.* **25**, 72–78.
54. Garcia-Junco-Clemente, P., Ikrar, T., Tring, E., Xu, X., Ringach, D.L., and Trachtenberg, J.T. (2017). An inhibitory pull-push circuit in frontal cortex. *Nat. Neurosci.* **20**, 389–392.
55. Brooks, P.L., and Peever, J. (2016). A Temporally Controlled Inhibitory Drive Coordinates Twitch Movements during REM Sleep. *Curr. Biol.* **26**, 1177–1182.
56. Stahl, J.S. (2004). Using eye movements to assess brain function in mice. *Vision Res.* **44**, 3401–3410.
57. Sánchez-López, A., and Escudero, M. (2011). Tonic and phasic components of eye movements during REM sleep in the rat. *Eur. J. Neurosci.* **33**, 2129–2138.
58. Fulda, S., Romanowski, C.P., Becker, A., Wetter, T.C., Kimura, M., and Fenzel, T. (2011). Rapid eye movements during sleep in mice: high trait-like stability qualifies rapid eye movement density for characterization of phenotypic variation in sleep patterns of rodents. *BMC Neurosci.* **12**, 110.
59. Bierman, A., Figueiro, M.G., and Rea, M.S. (2011). Measuring and predicting eyelid spectral transmittance. *J. Biomed. Opt.* **16**, 067011.

60. Sharon, O., and Nir, Y. (2017). Attenuated fast steady-state visual evoked potentials during human sleep. *Cereb. Cortex*. Published online February 25, 2017. <https://doi.org/10.1093/cercor/bhx043>.
61. McCormick, D.A., and Bal, T. (1994). Sensory gating mechanisms of the thalamus. *Curr. Opin. Neurobiol.* *4*, 550–556.
62. Sela, Y., Vyazovskiy, V.V., Cirelli, C., Tononi, G., and Nir, Y. (2016). Responses in Rat Core Auditory Cortex are Preserved during Sleep Spindle Oscillations. *Sleep* *39*, 1069–1082.
63. Walker, M.P., and Stickgold, R. (2004). Sleep-dependent learning and memory consolidation. *Neuron* *44*, 121–133.
64. Jacobs, G.H., Williams, G.A., and Fenwick, J.A. (2004). Influence of cone pigment coexpression on spectral sensitivity and color vision in the mouse. *Vision Res.* *44*, 1615–1622.
65. Xu, M., Chung, S., Zhang, S., Zhong, P., Ma, C., Chang, W.C., Weissbourd, B., Sakai, N., Luo, L., Nishino, S., and Dan, Y. (2015). Basal forebrain circuit for sleep-wake control. *Nat. Neurosci.* *18*, 1641–1647.

STAR★METHODS

KEY RESOURCES TABLE

REAGENT or RESOURCE	SOURCE	IDENTIFIER
Chemicals, Peptides, and Recombinant Proteins		
Tropicamidum, % 0.5	Thea Pharma	Tropicamide 0.5% SDU Faure
Dapiprazole, % 0.5	Angelini	Glamidolo
Experimental Models: Organisms/Strains		
Mouse: C57BL/6	Charles River Laboratories	C57BL/6J
Software and Algorithms		
Electrophysiology acquisition interface	Open-ephys.org	Open Ephys GUI
Other		
USB camera, 0.3MP Mono Firefly MV USB	Point Grey Research	FMVU-03MTM
Micro-video lens, 25.0 mm FL, No IR-Cut Filter, f/2.5	Edmund Optics	#56-776
LED, 940 nm 5mm T-1 3/4	Everlight Electronics	IR323
Electrophysiology acquisition board	Open-ephys.org	Acquisition board
Headstage, 32 channels	Intan Technologies	RHD2132/RHD2216
ECoG wires, 75 μ m	Science Products	AU-3T
EMG wires, 75 μ m	Science Products	SS-2T/HH

CONTACT FOR REAGENT AND RESOURCE SHARING

Further information and requests for resources and reagents should be directed to and will be fulfilled by the Lead Contact, Daniel Huber (daniel.huber@unige.ch).

EXPERIMENTAL MODEL AND SUBJECT DETAILS

Seven wild-type (C57BL/6, 10 to 11 week old) male mice were used for this study. Animals were caged individually, kept at 12 hr dark/light cycle and were placed under a water restriction regime (1 mL/day). The habituation sessions and experiments were performed in the second tierce of the light period. All procedures were reviewed and approved by the local ethics committee and the authorities of the Canton Geneva.

METHOD DETAILS

Surgeries

To implant the titanium frame for head-fixation, mice were anesthetized with 2% isoflurane-oxygen mix and kept warm on a heating pad (T/PUMP, TP500C). Injections of carprofen (Rimadyl, 50 mg/mL, 1:20 dilution in NaCl, 50 μ L sub-cutaneous), buprenorphine (Temgesic, 0.3 mg/mL 1:2 dilution in NaCl 25 μ L intramuscular) and dexamethasone (Mephamesone-4, 4 mg/mL, 20 μ L intramuscular) were given. The eyes were covered with Vaseline. Local anesthetic lidocaine (Rapidocain 10 mg/mL, 50 μ L subcutaneous) was applied to the scalp before removal. A titanium head bar was glued to the dried skull with cyanoacrylic glue (ergo 5300 elastomer). Small craniotomies for the ECoG electrodes were drilled over primary motor cortex (in right hemisphere 1.5 mm lateral (L), 1.5 mm rostral (R) of bregma) and cerebellum (all animals, midline 6 mm R). Custom electrodes for ECoG recordings were made from Teflon coated gold wires (75 μ m, AU-3T, Science Products). The electrodes were soldered to a miniature connector (Millmax). For EMG recordings, custom electrodes were fabricated with twisted Teflon coated half hard stainless steel wires (75 μ m, SS-2T/HH, Science Products). The coating of the EMG electrodes was stripped off with sharp tweezers and used as bipolar electrodes. These wires were guided into the neck muscles with a 24 G needle and immobilized in the muscle by bending the ends to a hook. Finally, the electrodes and the titanium frame were covered with transparent dental acrylic (Lang Dental Ortho-Jet Powder B1320). The animals were taken off the anesthesia, left to recover in a clean cage placed on a heating pad for 2 hr. Recordings started after an additional recovery period of 7 to 10 days.

Handling and sleep training

Animals were handled for 10 min per day for 6 consecutive days. To habituate the mice to sleep under head-fixed condition, their body was placed in a small plastic box (80x80x50 mm) which was filled with cotton bedding to comfortably accommodate the

animal's body. The head of the animals was kept at a 30° angle to imitate the natural sleep position in during head fixation (Figure 1C). During habituation and recordings the mice were held in a sound and light isolated Faraday cage. Through the first three sessions the mice were kept head-fixed for 10, 20 and 30 min and were delivered random water rewards through a lick port. In later sessions water delivery period remained 30 min while the duration of the head fixation increased by 20 to 30 min reaching to ~4 h in 10 to 12 sessions. The state of the mouse was continuously monitored with an IR USB camera (Point Grey Firefly MV USB FMVU-03MTM).

X-Ray imaging

X-Ray imaging to determine the body position during different head-fixed conditions was conducted using a custom lead shielded BV-25 (Philips) X-Ray machine equipped with a 120 × 70 mm CMOS detector (1207, Dexela). The X-Ray source was run at 52 kV. The effective dose in the path was determined with a RadeEye B20 Geiger counter (Thermo Scientific) and the cumulative dose during the lifetime was kept below 10mSv per animal. Images were acquired and analyzed using custom MATLAB code. During the X-Ray imaging the mice were continuously monitored with an IR USB camera (Point Grey Firefly MV).

Electrophysiology

ECoG and EMG data were acquired at 1 kHz using a 16 (for natural sleep recordings in the home cage) or 32 channel head stage (for head-fixed recordings) (RHD2132/RHD2216 Amplifier Board, OpenEphys). The signals from the ECoG electrode were referenced to the cerebellar electrode and the bipolar EMG channels were subtracted from each other. Signals were high-pass filtered at 0.1 Hz and a Fast Fourier Transform (FFT) was used to calculate the power spectrum of the ECoG and EMG signals with a 2 s sliding window sequentially shifted in 0.1 s increments. Each 2 s interval of data was first multiplied by an equal length Hamming window before applying the FFT. For the analysis of natural sleep recordings cortical electrodes were referenced to their contralateral counterparts to eliminate movement artifacts on the ECoG signal.

Heart beat detection

Heart rate was extracted from the EMG signal by detecting the prominent biphasic pulses (≈ 10 ms duration) occurring rhythmically. For this purpose, the EMG signal was filtered between 30 and 300 Hz and heart pulses were detected with the *findpeaks* MATLAB function applied to the squared absolute values of the filtered signal. Heart rate was computed by binning the pulse times into 1 s bins and calculating the mean of the inter-pulse-interval inverse values for each bin. Heart rate was up-sampled to the time base of pupil size by linear interpolation before calculating the cross-correlation between their Z-scored values.

Pupil tracking with iBip

Pupils of both eyes were monitored with two separate digital USB cameras (Point Grey Research 0.3MP Mono Firefly MV USB FMVU-03MTM) and acquired and saved at 10 frames/s (240×376 pixels 8-bit greyscale images) with a custom video acquisition system written in MATLAB. The timestamp of each frame relative to a digital trigger were saved in the image headers and used for post hoc alignment of pupil and electrophysiology data. To obtain high contrast images of the pupil we used infrared back-illumination pupillometry (iBip). iBip consists of a 940 nm LED (Everlight Electronics, 3 mW, 40 mA, 1.2 V) positioned on the skull above frontal cortex. Light reached the head through the polished dental acrylic of the head-cap. Light emission to the side of the LED was blocked with black tape shielding. The LED at this intensity level did not produce any additional heating of the illuminated area (measured by Peaktech 5140 digital thermometer).

Pharmacology and light stimulation experiments

Before the start of the recording session, one eye of the mouse was instilled with a drop of cholinergic receptor antagonist Tropicamide (Tropicamide, Thea Pharma, ~ 100 μ L, 0.5%) or the alpha receptor antagonist Dapiprazole (Glamidolo, Angelini, ~ 100 μ L, 0.5%), while the other eye was left intact ($n = 7$ mice). Animals were given 1 to 2 days of break in between pharmacological experiments. The side of the drugged eye was switched every session. For the light stimulation experiments a LED light source (510 nm, 90 μ W) was positioned 20 mm in front of each eye ($n = 2$ mice). 510 nm wavelength was chosen as the center of the mouse green cone spectrum [64] and the 90 μ W were found to be sufficient to induce changes in the ECoG bands (as determined in pilot experiments). The LEDs were mounted in 5 mm wide black tubes to restrict illumination to the targeted eye only. Light pulses (1 s) were triggered manually during NREM sleep when the control pupil diameter was in a decreasing phase and reached ~ 0.5 mm.

QUANTIFICATION AND STATISTICAL ANALYSIS

Sleep state classification

Sleep classification was carried out semi-automatically in several consecutive steps. First, delta and theta power signals were calculated by summing the ECoG power in the 1 to 4 Hz, and 6 to 10 Hz frequency ranges, respectively. The EMG power was summed in the ranges between 30 and 300 Hz. NREM sleep was identified by 50 s uninterrupted periods where delta power was two standard deviations larger than its mean and EMG power smaller than its mean (similar to [65]). A state was marked as REM sleep when the theta/delta ratio was two standard deviations larger than its mean and EMG power was two standard deviations smaller than its mean. Everything else was marked as awake. All sleep stages were proof read and corrected by two experienced observers. Micro

awakenings during NREM were identified manually and marked as awake. NREM bouts that were interrupted by micro awakenings were considered continuous. All analysis was carried out with custom MATLAB scripts.

Pupil diameter detection

To extract the pupil diameter, single frame images were first centered on and cropped around the pupil (90x90 pixels). The greyscale pixel values of the cropped image were classified into 2 clusters (dark and bright pixels) using K-means clustering. A binary image, obtained by setting the dark pixels to 0 and the bright pixels to 1, was used to find connected components (bwconncomp function in MATLAB) and the largest component was deemed to correspond to the pupil. An ellipse was fit to the component's contour (linear least-squares fitting) and its major axis was defined to be the pupil diameter. Eye blinks and periods with closed eyelids were manually detected and excluded from analysis. The pupil diameter traces were upsampled to 1 kHz by linear interpolation to match the ECoG signal sampling and low pass filtered at 2 Hz (except for light stimulation experiments). Converting pupil size to mm was done by calibrating the images to a video recording of 1 mm square graph paper.

Pupil-based sleep state classification

A neural network with one hidden layer was used to classify sleep states based on pupil diameter. For each sleep session classification, the network was first trained on data from all other sessions ($n = 5$ mice). Training trials consisted of 100 s pupil diameter traces (sampled at 10 Hz) at the input layer and the corresponding sleep state label at the output layer (awake, REM or NREM). Sleep bouts that were shorter than 100 s were omitted in this analysis. The hidden layer size was set to 30 nodes. The trained network coefficients were then used to predict sleep states of the session not used for training. Prediction accuracy was calculated as the % of the 100 s trials correctly classified in each session and separately for each of the three sleep states.

Relating ECoG oscillations to pupil size fluctuations

The recorded ECoG signals of each session were bandpass filtered into the traditional delta (1 to 4 Hz), theta (4 to 7 Hz), alpha (7 to 14 Hz), beta (15 to 30 Hz), low (30 to 60 Hz) and high gamma (60 to 100 Hz) frequency bands using a bidirectional second order Butterworth filter, thus eliminating possible phase shifts introduced by filtering. The frequency definitions correspond to cut-off values at -3 dB attenuation. The instantaneous amplitude of each bandlimited oscillation was obtained by computing the magnitude of its Hilbert transform. To assess how the magnitude of cortical oscillations changes relative to fluctuations in pupil size, Pearson's correlation (R) was calculated between the low-pass filtered (bidirectional single pole IIR filter, i.e., exponential decay impulse response) Hilbert amplitude signals and pupil diameter. For each frequency band, the time constant of the low pass filter that maximized $|R|$ was evaluated for each sleep state separately (fminsearch function in MATLAB, $n = 5$ mice).

We used general linear modeling (GLM) to assess the extent to which ECoG oscillations of each band can be used to model changes in pupil diameter. The GLM consisted of two regressors: the filtered ECoG oscillatory amplitude and a constant term. The former trace was first standardized by taking its z-score. The low pass filter time constant and the two GLM coefficients that minimized the sum of squared errors between the fitted and actual pupil diameter were evaluated on half of the data in each session. The other half of the data, not used for parameter fitting, was used to validate the prediction by computing the explained variance as $1 - \text{var}(p_m - p_{pr}) / \text{var}(p_m)$ where p_m is the measured and p_{pr} the predicted pupil diameter and $\text{var}()$ symbolizes the signal's variance.

The spectral content, in the infra-slow frequency range, of pupil fluctuations and bandlimited ECoG oscillation amplitude changes during NREM sleep (Figures S2E–S2G) was obtained using the Fast Fourier Transform (FFT). Hilbert transforms of the bandpass filtered ECoG signals or the pupil diameter trace were first normalized to their respective mean values for each NREM bout separately and then multiplied by an equal length Hamming window. The traces were padded with zeros for the number of FFT points to be equal to a higher power of 2. The obtained absolute FFT values were first interpolated at a 0.001 Hz frequency resolution and then averaged across all NREM bouts of an experimental session.

Changes in ECoG signals with light stimulation

For light stimulation experiments, % change was calculated with respect to a 10 s baseline preceding stimulus onset. Drug and control conditions were compared (red and blue traces in Figures 4C–4F) based on mean values of a 20 s post stimulation period.